CHAPTER 3

BEAM-WAVE INTERACTION ANALYSIS OF THE SCC STRUCTURE

3.1. Overview

3.2. Introduction

3.3. Analysis

3.3.1. EM-Field Expression in the Presence of Electron Beam

3.3.2. Boundary Condition

3.3.3. Dispersion Relation

3.3.4. Temporal Growth Rate

3.4. Result and Discussion

3.4.1. Parametric Study of the Temporal Growth Rate

3.4.2. Validation of the Derived Analytical Relation

3.5. Conclusion

CHAPTER 3

BEAM-WAVE INTERACTION ANALYSIS OF THE SCC STRUCTURE

3.1. Overview

In this chapter, the EM behavior of the SCC structure intersecting with an electron beam is accomplished with the help of the field matching approach for the transverse magnetic (TM) modes. Vlasov-Maxwell's equation has been used to analyze the region where the electron beam is present. To find out the RF behavior of the SCC structure, the effect of all harmonics present within the structure is considered during the calculation of its dispersion relation. This analysis is further extended to assess the operating frequency and temporal growth of the structure. Also, the effect of the different beam parameters on the temporal growth rate behavior is analyzed. To validate the proposed theoretical analysis, the structure is simulated with the help of commercial "CST Studio Suite" code, and the obtained simulated dispersion curve is compared with the analytically obtained dispersion curve; for the special case (i.e. $r_e = 0$).

3.2. Introduction

Due to wide potential applications of the HPM oscillators in various domains, such as food irradiation, materials processing, cargo inspection, nuclear physics, high energy colliders, nuclear waste management (radioisotope production), linear accelerators, and others [Knapp *et al.* (1965), Knapp *et al.* (1976), Miller (2006), Hamm *et al.* (2012)]. Therefore, to ensure the efficient operation of the microwave oscillators, it is essential to know the behavior of its key assemblies. The most crucial component of any microwave oscillator system is its RF interaction cavity, so knowing its behavior in the presence of

the electron beam is very necessary. A dispersion relation is an excellent tool that provides the RF behavior of any RF interaction structure and highlights its structural dependency which is very helpful to the design engineers to develop a better understanding of the device and development of the system.

To understand its working mechanism a very few pieces of literature is reported till now. Knapp *et al.* reported an equivalent circuit analysis of SCC to describe the EM behavior (i.e. resonance mode and operating frequency) of the SCC [Knapp *et al.* (1965)]. In this study, research focuses on the calculation of the dispersion relation of the structure, which incorporates the effect of magnetic coupling while ignoring the effect of electric coupling. In addition, the effect of harmonics on the dispersion relation is also not included. The calculation of its interaction impedance is also absent in their analysis. Tripathi *et al.* performed the EM analysis of the SCC structure in the absence of electron beam, which included the effect of both types of coupling (i.e. magnetic and electric coupling) and all the harmonics present within the structure [Tripathi *et al.* (2020)]. The effect of various structural parameters of the SCC structure on the dispersion characteristic and interaction impedance is also studied in their analysis [Tripathi *et al.* (2020)]. But the RF behavior of the SCC is still untouched.

Since there is no literature available that explains the RF behavior of the structure, therefore it becomes extremely important that a study be carried out to develop a better understanding of the SCC's behavior in the presence of the electron beam. Therefore in this chapter, the RF behavior of the SCC structure has been investigated with the help of the field matching approach. In this analysis, the expression of the dispersion relation for the transverse magnetic (TM) mode is obtained in the presence of an electron beam and

then the effect of the different beam radii on the dispersion characteristics has been investigated. The dispersion relation of the SCC in the presence of an electron beam also provides information regarding the temporal growth rate of the device.

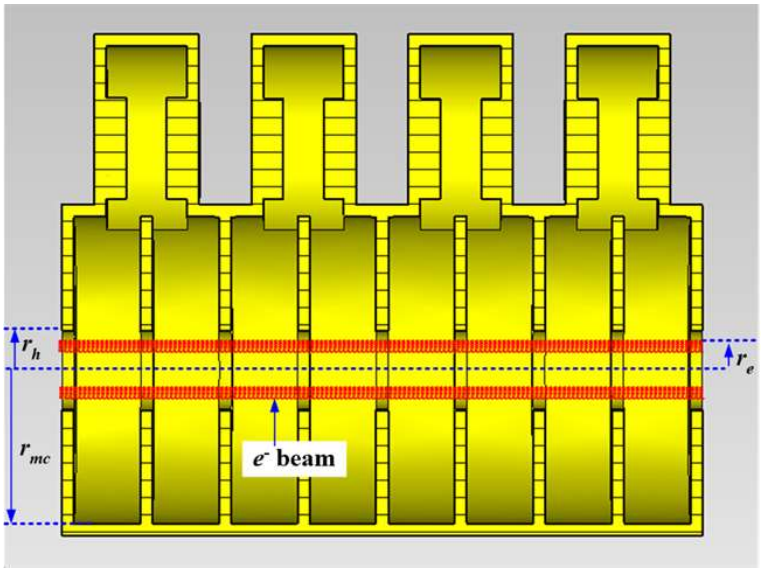

Figure 3.1: Schematic of periodic SCC structure in the presence of electron beam.

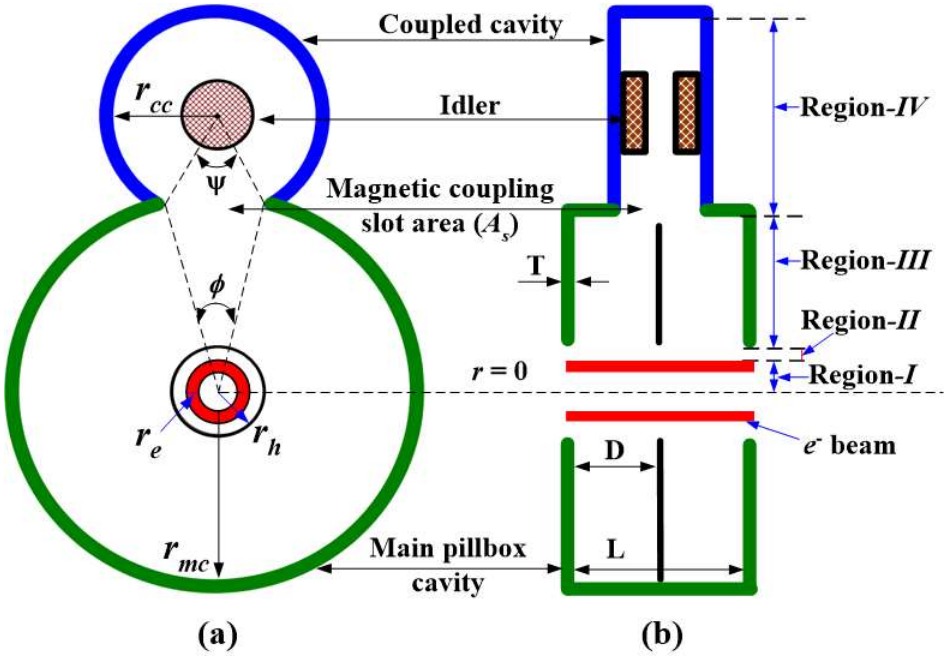

Figure 3.2: Different cross-section views of the unit cell of the SCC structure: (a) lateral cross-section view, and (b) longitudinal cross-section view.

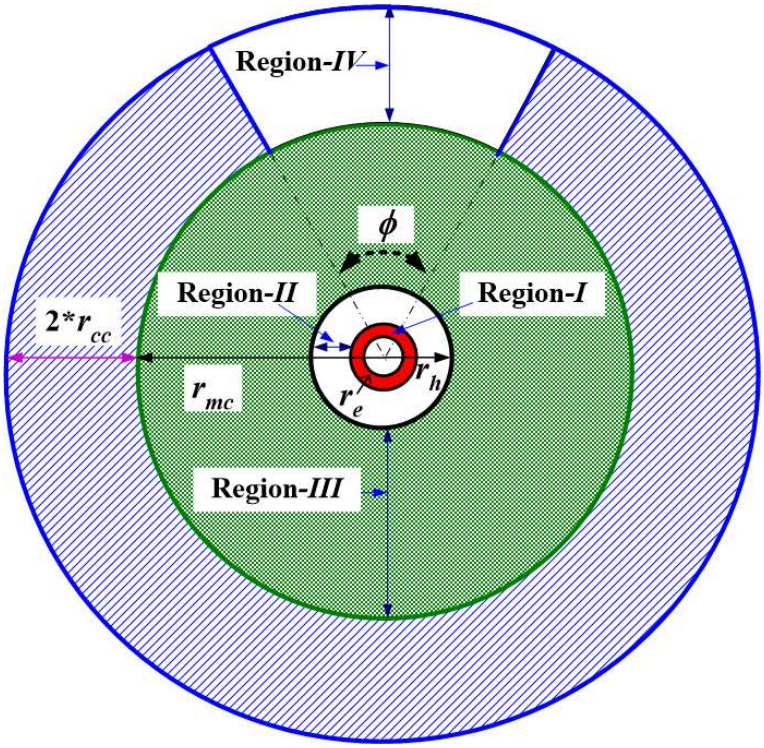

Figure 3.3: The proposed equivalent model of the SCC structure for the RF analysis.

3.3. Analysis

Fig. 3.1, shows the periodic nature of the SCC structure while Fig. 3.2 shows the different cross-section views of the unit cell of SCC structure i.e. Fig. 3.2 (a) shows the lateral cross-section view, and Fig. 3.2 (b) shows the longitudinal cross-section view**.** For the RF analysis, an equivalent model shown in Fig. 3.3 has been considered. Tripathi *et al.* proposed this equivalent model for the SCC structure and validated this structure by comparing the results obtained from EM analysis with the results obtained from the simulation tool i.e. CST Studio Suite [Tripathi *et al.* (2020)]. According to Floquet's theorem unit cell of the any periodic structure is sufficient for the analysis. The unit cell of the SCC is divided into four regions; Region-*I* (i.e. electron occupied region $\left(0 \le r \le r_e\right)$), Region-*II* (i.e. free space region $\left(r_e < r \le r_h\right)$), Region-*III* (i.e. disc occupied region

$\left(r_h < r \le r_{mc}\right)$), and finally Region-*IV* (i.e. coupled-cavity region $\left(r_{mc} < r \le \left(r_{mc} + 2\times r_{cc}\right)\right)$). Before calculating the field expressions in a different region of the SCC, it is assumed that Region-*II* supports the traveling waves, while Region-*III* and Region-*IV* support the standing waves, and the EM fields are time-independent. It is also assumed that the axial periodicity of the SCC introduces the space harmonics of the traveling wave, while reflections of EM waves from the metallic surfaces introduces the modal harmonics of the standing wave [Lemke (1989), Singh *et al.* (2004), Yue *et al.* (2004), Tripathi *et al.* (2020)]. The superscript *I*, *II*, *III*, and *IV* associated with the different parameters shows that the parameter belongs to Region *I*, *II*, *III*, and *IV*, respectively.

3.3.1. EM-Field Expression in the Presence of Electron Beam

For the analysis, the cylindrical coordinate system $\left(r,\theta,z\right)$ is considered here, to characterize the symmetric TM_{0m} mode (i.e. $H_z = 0$). The relevant EM fields for *TM* mode are radial electric field intensity $\left(E_r\right)$, azimuthal electric field intensity $\left(E_\theta\right)$, axial electric field intensity $\left(E_z\right)$, radial magnetic field intensity $\left(B_r\right)$, and azimuthal magnetic field intensity $\left(B_\theta\right)$. The EM field expression in the presence of an electron beam for *TM* mode can be expressed using Vlasov-Maxwell's equation. Vlasov's equation is mainly used to describe the electron beam dynamics in a collision-less state. The EM field expression for beam presence condition can be given as [Lemke (1989), Basu (1995), Singh *et al.* (2004), Yue *et al.* (2004), Amin and Ogura (2007), Dwivedi and Jain (2012)]:

$$\left(\frac{\partial}{\partial t} + v_z \frac{\partial}{\partial z}\right) P_z = -eE_z^I \tag{3.1}$$

$$\frac{1}{r}\frac{\partial}{\partial r}\left(rE_r^I\right)+\frac{\partial E_z^I}{\partial z}=-4\pi en_e \tag{3.2}$$

$$\frac{\partial E_r^I}{\partial z}-\frac{\partial E_z^I}{\partial r}=-\frac{1}{c}\frac{\partial B_\theta^I}{\partial t} \tag{3.3}$$

$$-\frac{\partial B_\theta^I}{\partial z}=\frac{1}{c}\frac{\partial E_r^I}{\partial t} \tag{3.4}$$

$$\frac{1}{r}\frac{\partial(rB_\theta^I)}{\partial z}=\frac{4\pi}{c}J_z+\frac{1}{c}\frac{\partial E_z^I}{\partial t} \tag{3.5}$$

Where $P_z\left(=\gamma m_e v_z\right)$ is the axial momentum, $\gamma\left(=1/\left(1-v_z^2/c^2\right)\right)^{1/2}$ is the relativistic factor, $J_z\left(=-\eta en_e v_z\delta\left(r-r_e\right)\right)$ is the axial current density, n_e is the charge number density, v_z is the axial drift velocity, $\delta\left(r-r_e\right)$ is the delta function, and r_e is the electron beam radius. The parameter η is the normalized factor determined by $\eta\left(=|I_e|/\left(2\pi er_e n_e v_z\right)\right)$. Solving the above equation, the field components for the *TM* mode are:

$$E_{r,m}^I=i\frac{\beta_m^I}{\left(\Gamma_m^I\right)^2}\frac{dE_{z,m}^I}{dr} \tag{3.6}$$

$$B_{\theta,\mathrm{m}}^I=i\frac{\omega/c}{\left(\Gamma_m^I\right)^2}\frac{dE_{z,\mathrm{m}}^I}{dr} \tag{3.7}$$

$$\left(\frac{1}{r}\frac{d}{dr}r\frac{d}{dr}+\left(\Gamma_m^I\right)^2\right)E_{z,\mathrm{m}}^I=\frac{\alpha c^2}{(\pi/2)r_e}\frac{\left(\Gamma_m^I\right)^2E_{z,\mathrm{m}}^I}{(\omega-v_z\beta_m^I)^2}\delta(r-r_e) \tag{3.8}$$

where $\Gamma_m^I=\sqrt{\left(k_c\right)^2-\left(\beta_m^I\right)^2}$ is the radial propagation constant with $k_c=\left(\frac{\omega}{c}\right)$, and $\alpha\left(=\pi|I_e|/\left(\gamma_0^2I_A\right)\right)$ with $I_A\left(=17.1\gamma v_z/c\right)$ kA.

(a) Field expressions for Region-*I* (i.e. $0 \le r \le r_e$)

$$E_z^I = \sum_{p=-\infty}^{\infty} \sum_{m=-\infty}^{\infty} \left(A_{p,m}^* J_p(\Gamma_m^* r) \right) \times \exp\left\{ -j\left(\beta_m^I z + p\phi \right) \right\} \tag{3.9}$$

$$H_\phi^I = \sum_{p=-\infty}^{\infty} \sum_{m=-\infty}^{\infty} \left(\frac{-j\omega\varepsilon}{\Gamma_m^*} \right) A_{p,m}^* J'_{p,m}\left(\Gamma_m^* r \right) \times \exp\left\{ -j\left(\beta_m^I z + p\phi \right) \right\} \tag{3.10}$$

where $\beta_m^I \left(= \beta_0 + 2m\pi / L \right)$ is the axial propagation constant, Γ_m^* is the radial propagation constant in presence of an electron beam i.e. $\Gamma_m^* = \Gamma_m^I \sqrt{\left(1 - \left(\left(\alpha c^2 / (\pi/2) r_e (\omega - v_z \beta_m^I)^2 \right) \times \delta(r - r_e) \right) \right)}$, where $\Gamma_m = \sqrt{\left(k_c \right)^2 - (\beta_m^I)^2)}$. The $A_{p,m}^*$ is the undetermined coefficient; $m = 0, \pm 1, \pm 2, \pm 3, ...,$ $p = 0, \pm 1, \pm 2, \pm 3, ...,$ J_p is the Bessel function of 1st kind of order *p*.

(b) Field expressions for Region-*II* (i.e. $r_e < r \le r_h$)

By considering all the space harmonics present in Region-*II*, the expression for the axial electric field is written as [Lemke (1989), Basu (1995), Singh *et al.* (2004), *et al.* (2004), Amin and Ogura (2007), Dwivedi and Jain (2012)]:

$$E_z^{II} = \sum_{p=-\infty}^{\infty} \sum_{m=-\infty}^{\infty} \left(A_{p,m}^{II} J_p\left(\Gamma_m^{II} r \right) + B_{p,m}^{II} Y_p\left(\Gamma_m^{II} r \right) \right) \times \exp\left\{ -j\left(\beta_m^{II} z + p\phi \right) \right\} \tag{3.11}$$

where, $\beta_m^{II} \left(= \beta_0 + 2m\pi / L \right)$ is the axial propagation constant, $\Gamma_m^{II} \left(= \sqrt{\left(k_c \right)^2 - \left(\beta_m^{II} \right)^2} \right)$ is the radial propagation constant, $k_c = \left(\frac{\omega}{c} \right)$ is the free space propagation constant, $p \left(= \beta_\varphi^{II} = 0, \pm 1, \pm 2, \pm 3, ... \right)$ is the azimuthal mode number, $J_p\left(\Gamma_m^{II} r \right)$,

$m\left(=0,\pm1,\pm2,\pm3,.....\right)$ is the number of space harmonics, $J_p(\Gamma_m^{II} r)$ and $Y_p(\Gamma_m^{II} r)$ the Bessel's function of the first kind and second kind, respectively.

The azimuthal magnetic field in Region-*II* is obtained by using Maxwell's equation [Lemke (1989), Basu (1995), Singh *et al.* (2004), *et al.* (2004), Amin and Ogura (2007), Dwivedi and Jain (2012)]:

$$H_\phi^{II} = \sum_{p=-\infty}^{\infty}\sum_{m=-\infty}^{\infty}\left(\frac{-j\omega\varepsilon}{\Gamma_m^{II}}\right)\left\{A_{p,m}^{II} J_p'\left(\Gamma_m^{II} r\right) + B_{p,m}^{II} Y_p'\left(\Gamma_m^{II} r\right)\right\}\times\exp\left\{-j\left(\beta_m^{II} z + p\phi\right)\right\} \quad (3.12)$$

where, prime sign attached with the parameters indicates its differentiation with respect to '*r*'.

(c) Field expressions for Region-*III* (i.e. $r_h < r \le r_{mc}$)

In Region-*III*, the standing EM waves are formed due to the reflection of EM waves from the metallic surfaces. Since the standing wave have both the components i.e. forward and backward components, the axial electric field (i.e. E_z^{III}) can be written as [Lemke (1989), Basu (1995), Singh *et al.* (2004), *et al.* (2004), Amin and Ogura (2007), Dwivedi and Jain (2012)]:

$$E_z^{III} = \sum_{p=-\infty}^{\infty}\sum_{n=1}^{\infty}\left(A_{p,n}^{III} J_p\left(\Gamma_n^{III} r\right) + B_{p,n}^{III} Y_p\left(\Gamma_n^{III} r\right)\right)\times\sin\left(\beta_n^{III} z\right)\exp\left(-jp\phi\right) \quad (3.13)$$

Furthermore, the azimuthal magnetic field can be obtained with the help of Maxwell's equation, we get:

$$H_\phi^{III} = \sum_{p=-\infty}^{\infty}\sum_{n=1}^{\infty}\left(\frac{-j\,\omega\varepsilon}{\Gamma_n^{III}}\right)\left(A_{p,n}^{III} J_p'\left(\Gamma_n^{III} r\right) + B_{p,n}^{III} Y_p'\left(\Gamma_n^{III} r\right)\right)\times\sin\left(\beta_n^{III} z\right)\exp\left(-jp\phi\right) \quad (3.14)$$

(d) Field expressions for Region-*IV* (i.e. $r_{mc} < r \le (r_{mc} + 2 \times r_{cc})$)

The axial electric field intensity in the Region-*IV* (i.e. coupling-cavity region) can be expressed as [Singh *et al.* (2004)]:

$$E_z^{IV} = \sum_{\nu=1}^{\infty} \sum_{q=1}^{\infty} \left(A_{\nu,q}^{IV} X_q(r) \right) \sin\left(\beta_q^{IV} z \right) \sin(\nu\phi) \tag{3.15}$$

where,

$$X_q(r) = \left(Y_\nu\left(\Gamma_q^{IV} r \right) Y_\nu\left(\Gamma_q^{IV} (r_{mc} + 2r_{cc}) \right) - J_\nu\left(\Gamma_q^{IV} (r_{mc} + 2r_{cc}) \right) Y_\nu\left(\Gamma_q^{IV} r \right) \right) \tag{3.16}$$

where, $\Gamma_q^{IV} \left(= \sqrt{(k_c)^2 - \left(\beta_q^{IV} \right)^2} \right)$ is the radial propagation constant, $\beta_q^{IV} \left(= q\pi / (L - T) \right)$ is the axial propagation constant, and $q \left(= 1, 2, 3, ... \right)$ is the number of the modal harmonic associated with the standing wave in Region-*IV*. The radial electric field and azimuthal magnetic field for the Region-*IV* is obtained by using Maxwell's equation, and expressed as [Singh *et al.* (2004), Yue *et al.* (2004), Amin and Ogura (2007), Dwivedi and Jain (2012)]:

$$E_r^{IV} = \sum_{\nu=1}^{\infty} \sum_{q=1}^{\infty} \left(\frac{-j\beta_q^{IV}}{\Gamma_q^{IV}} \right) \left(A_{\nu,q}^{IV} X_q'(r) \right) \times \cos\left(\beta_q^{IV} z \right) \sin(\nu\phi), \tag{3.17}$$

$$H_\phi^{IV} = \sum_{\nu=1}^{\infty} \sum_{q=1}^{\infty} \left(\frac{-j\,\omega\varepsilon}{\Gamma_q^{IV}} \right) \left(A_{\nu,q}^{IV} X_q'(r) \right) \times \sin\left(\beta_q^{IV} z \right) \sin(\nu\phi) \tag{3.18}$$

where, $X'_q(r)$ is the differentiation of $X_q(r)$ with respect to '*r*', and $X'_q(r)$ is given as:

$$X_q'(r) = \left(J_\nu'\left(\Gamma_q^{IV} r \right) Y_\nu\left(\Gamma_q^{IV} (r_{mc} + 2r_{cc}) \right) - J_\nu\left(\Gamma_q^{IV} (r_{mc} + 2r_{cc}) \right) Y_\nu'\left(\Gamma_q^{IV} r \right) \right) \tag{3.19}$$

3.3.2. Boundary Condition

The corresponding periodic structure has three discontinuities i.e. between Region-*I* and Region-*II* (i.e. $0 \le z \le L \quad at \quad r = r_e$), between Region-*II* and Region-*III* (i.e. $0 \le z \le L \quad at \quad r = r_h$), and between Region-*III* and Region-*IV* (i.e. $-\phi/2 \le \theta \le +\phi/2 \quad at \quad r = r_{mc}$). According to the theorem of continuity, the tangential component must be continuous at the discontinuity therefore, the axial electric field and the azimuthal magnetic field should be continuous at the discontinuity, and the electric field should be zero at the metal boundary. Therefore, the EM boundary conditions for this structure can be written as:

(a) For Region *III* and *IV*

$$E_z^{III} = \begin{cases} E_z^{IV} & -\phi/2 \le \theta \le +\phi/2 \quad at \quad r = r_{mc} \\ 0 & elsewhere \end{cases} \tag{3.20}$$

$$H_\phi^{III} = H_\phi^{IV} \quad -\phi/2 \le \theta \le +\phi/2 \quad at \quad r = r_{mc} \tag{3.21}$$

(b) For Region *II* and *III*

$$E_z^{II} = E_z^{III} \qquad 0 \le z \le L \quad at \quad r = r_h \tag{3.22}$$

$$H_\phi^{II} = H_\phi^{III} \qquad 0 \le z \le L \quad at \quad r = r_h \tag{3.23}$$

(c) For Region *I* and *II*

$$E_z^{I} = E_z^{II} \qquad 0 \le z \le L \quad at \quad r = r_e \tag{3.24}$$

The second boundary condition between beam present region and beam absent region can be obtained by multiplying expression (3.8) by rdr on both sides and integrating it from $r_e-\varsigma$ to $r_e+\varsigma$ consider $\varsigma / r_e \ll 1$. The obtained boundary condition is written as:

$$r\frac{d}{dr}E^{I}_{z,m}\Big|_{r_e-\varsigma}^{r_e+\varsigma}+\Gamma_m^2\int_{r_e-\varsigma}^{r_e+\varsigma} r\,dr\,E^{I}_{z,m}=\frac{2\alpha}{\pi}\frac{\Gamma_m^2c^2}{\Omega_m^2}E^{I}_{z,m}(r_e) \tag{3.25}$$

3.3.3. Dispersion Relation

In the process of calculating the dispersion relation of any periodic structure, firstly all the relevant EM field expressions present in different regions of the periodic structure are obtained. After obtaining the field expressions, we equate the field expressions with the help of appropriate EM boundary conditions. This gives a set of simultaneous series of equations in terms of field constants. The coefficient (i.e. field constants) of these simultaneous equations is arranged in the determinant form. Finally, the non-trivial solution is obtained by making this determinant equal to zero.

(a) For Region *III* and *IV*

Using the first boundary condition (i.e. expression (3.20)), we get:

$$A^{IV}_{\nu,q}=\sum_{p=-\infty}^{\infty}\left\{A^{III}_{p,n}J_p\left(\Gamma^{III}_n r_{mc}\right)+B^{III}_{p,n}Y_p\left(\Gamma^{III}_n r_{mc}\right)\right\}\times\left(\frac{2\pi}{X_{\nu,q}\left(r_{mc}\right)E_{IV,III}}\right) \tag{3.26}$$

where,

$$E_{IV,III}=\left[\int_{-\theta/2}^{+\theta/2}\sin(\nu\phi)\exp(jp\phi)\,d\phi\right] \tag{3.27}$$

Similarly, using the second boundary condition (i.e. expression (3.21)), we can get:

$$A_{\nu,q}^{IV} = \sum_{p=-\infty}^{\infty} \left(\frac{\Gamma_q^{IV}}{\Gamma_n^{III}} \right) \left\{ A_{p,n}^{III} J_p' \left(\Gamma_n^{III} r_{mc} \right) + B_{p,n}^{III} Y_p' \left(\Gamma_n^{III} r_{mc} \right) \right\} \times \left(\frac{\theta}{X_{\nu,q}' \left(r_{mc} \right) E_{IV,III}} \right) \tag{3.28}$$

Equating expressions (3.26) and (3.27), we get a relation between $B_{p,n}^{III}$ and $A_{p,n}^{III}$. It is expressed as:

$$B_{p,n}^{III} = S_{B,A}^{III} A_{p,n}^{III} \tag{3.29}$$

where,

$$S_{B,A}^{III} = \left(\frac{2\pi \times \Gamma_n^{III} J_p \left(\Gamma_n^{III} r_{mc} \right) X_{\nu,q}' \left(r_{mc} \right) - \theta \times \Gamma_q^{IV} J_p' \left(\Gamma_n^{III} r_{mc} \right) X_{\nu,q} \left(r_{mc} \right)}{\theta \times \Gamma_q^{IV} Y_p' \left(\Gamma_n^{III} r_{mc} \right) X_{\nu,q} \left(r_{mc} \right) - 2\pi \times \Gamma_n^{III} Y_p' \left(\Gamma_n^{III} r_{mc} \right) X_{\nu,q}' \left(r_{mc} \right)} \right) \tag{3.30}$$

(b) For Region *II* and *III*

Similarly, the relationship between the coefficient of Region *III* and *II* can be established and the transformation coefficient from $B_{p,n}^{II}$ and $A_{p,n}^{II}$ can be derived as:

$$B_{p,n}^{II} = S_{B,A}^{II} A_{p,n}^{II} \tag{3.31}$$

here,

$$S_{B,A}^{II} = \left(\frac{\left(\Gamma_n^{III} \right) J_p' \left(\Gamma_m^{II} r_h \right) \times \left\{ J_p \left(\Gamma_n^{III} r_h \right) + S_{B,A}^{III} Y_p \left(\Gamma_n^{III} r_h \right) \right\}}{\left(\Gamma_m^{II} \right) Y_p \left(\Gamma_m^{II} r_h \right) \times \left\{ J_p' \left(\Gamma_n^{III} r_h \right) + S_{B,A}^{III} Y_p' \left(\Gamma_n^{III} r_h \right) \right\}} \right. \\ \left. \frac{-\left(\Gamma_m^{II} \right) J_p \left(\Gamma_m^{II} r_h \right) \times \left\{ J_p' \left(\Gamma_n^{III} r_h \right) + S_{B,A}^{III} Y_p' \left(\Gamma_n^{III} r_h \right) \right\}}{-\left(\Gamma_n^{III} \right) Y_p' \left(\Gamma_m^{II} r_h \right) \times \left\{ J_p \left(\Gamma_n^{III} r_h \right) + S_{B,A}^{III} Y_p \left(\Gamma_n^{III} r_h \right) \right\}} \right) \tag{3.32}$$

Using the boundary condition (3.24), we get:

$$A_{p,\mathrm{m}}^{II} = \sum_{m=-\infty}^{\infty} U_{m,n}^{*} A_{p,m}^{I} \tag{3.33}$$

where,

$$U_{m,n}^{*} = \frac{J_p\left(\Gamma_m^I r_e\right)}{J_p\left(\Gamma_m^{II} r_e\right) + S_{B,A}^{II} Y_p\left(\Gamma_m^{II} r_e\right)} \tag{3.34}$$

Similarly, after applying the boundary condition (3.25), we get:

$$A_{p,\mathrm{m}}^{II} = \sum_{m=-\infty}^{\infty} V_{m,n}^{*} A_{p,m}^{I} \tag{3.35}$$

where,

$$V_{m,n}^{*} = \frac{\pi r_e \left(\omega - v_z \beta_m^I\right)^2 \times \Gamma_m^I J_p'\left(\Gamma_m^I r_e\right) + 2\alpha\left(\Gamma_m^I\right)^2 c^2 J_p\left(\Gamma_m^I r_e\right)}{\pi r_e \left(\Gamma_m^{II}\right)\left(\omega - v_z \beta_m^I\right)^2 \times \left\{J_p'\left(\Gamma_m^{II} r_e\right) + S_{B,A}^{II} Y_p'\left(\Gamma_m^{II} r_e\right)\right\}} \tag{3.36}$$

By equating the equation (3.33) and (3.35), we get:

$$\sum_{m=-\infty}^{\infty} \left(U_{m,n}^{*} - V_{m,n}^{*}\right) A_{p,m}^{I} = 0 \tag{3.37}$$

Expression (3.37), represents a system of the infinite homogeneous equation. For each value of '*n*', the nontrivial solution of these simultaneous equations can set equal to zero. The determinant formed by the coefficients of field constants that are set to zero represents the dispersion relation of the structure in the presence of the electron beam. Thus for TM_{0m} mode, the equivalent periodic structure beam present dispersion relation can be given as:

$$det\left|U_{m,n}^{*} - V_{m,n}^{*}\right| = 0 \tag{3.38}$$

3.3.4. Temporal Growth Rate

In the presence of an electron beam, the roots of dispersion relation explained in the above section (i.e. expression (3.38)) results in complex roots of frequency for a range of wavenumber. This range of wavenumber is mainly called the instability region and is

considered as the region between the cutting point of beam-line (i.e. defined by $\omega = \beta_0 v_e$) and slow space charge wave (slow SCW) line on dispersion curve [Lemke (1989), Basu (1995), Singh *et al.* (2004), Yue *et al.* (2004), Amin and Ogura (2007), Dwivedi *et al.* (2012)]. The beam-line is defined by $\omega = \beta_0 v_e$, here, v_e is the velocity of the electron beam due to the applied beam voltage. The slow SCW is defined by Lemke $\omega = \beta_0 v_{\text{slow\_sc}}$ where $v_{\text{slow\_sc}} = v_e\left(1 - \omega_p / (\omega_c \gamma_0^{1.5})\right)$. In the instability region, the slow SCW interacts with the RF wave supported by the structure and produces real as well as imaginary roots of the frequency. The real root of frequency (i.e. f_r) gives the oscillation frequency of RF wave whereas the imaginary root of frequency (i.e. f_i) gives the temporal growth rate (i.e. rate at which the oscillation frequency grows with time in the instability region). To find the magnitude of the temporal growth rate, the imaginary value of frequency (i.e. f_i) is calculated using expression (3.38). This imaginary frequency causes the exponential to grow of the RF signal i.e. $\left(e^{-i2\pi(f_r + i f_i)t}\right)$ with an increase in time [Sagor *et al.* (2017)].

3.4. Results and Discussion

The RF behavior of the periodic SCC structure has been analyzed with the help of Vlasov-Maxwell's equation using the field matching approach. The dispersion relation of the periodic SCC structure has been obtained. The dispersion relation is an excellent tool to estimate the RF wave propagation behavior and its temporal growth rate. The temporal growth rate provides information regarding the growth of the RF signal with respect to time within the structure.

For the typically selected beam parameters, i.e. beam voltage (V_e = 100 kV), beam

current ($I_e = 200$ A), electron beam radius ($r_e = 0.9$ mm), and design specifications i.e. main cavity radius ($r_{mc} = 38.9$ mm), coupled-cavity radius ($r_{cc} = 25.51$ mm), hole radius ($r_h = 10.00$ mm), disc thickness (T = 3.00 mm), and periodicity (L = 39.00 mm); a dispersion curve is plotted with the help of dispersion relation which is obtained from equation (3.38). The dispersion curve obtained with the typically selected beam and design parameter mentioned above is shown in Fig. 3.4.

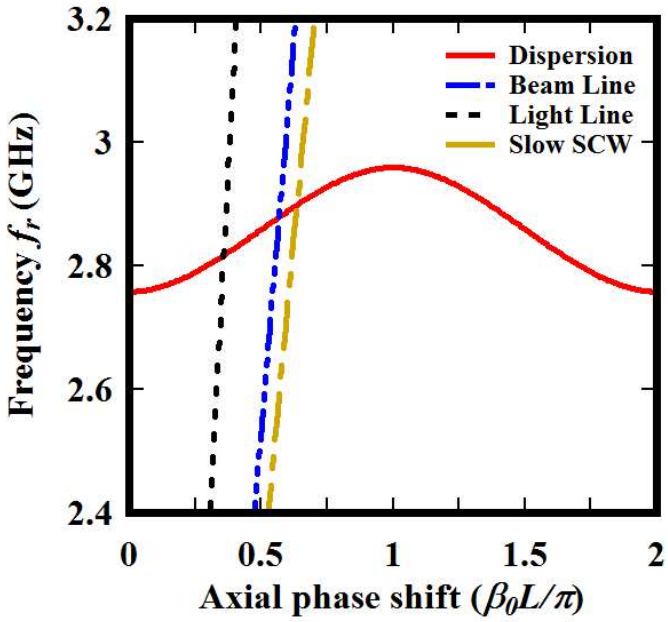

Figure 3.4: Dispersion curve of the periodic SCC structure in the presence of electron beam.

The fundamental mode of periodic SCC structure is TM_{01} mode. The region between light-line and beam-line is considered as an instability region and the temporal growth rate is calculated in this region. Fig. 3.5 shows the temporal growth rate (f_i) at different phases $(\beta_0 \times L)$ in radian for TM_{01} mode. From Fig. 3.5, that the maximum value of temporal growth rate for TM_{01} mode is ~0.062 per *ns* which specifies that frequency associated with

f_i (i.e. fundamental resonating mode frequency) increases rapidly as compared to the other resonating mode frequency.

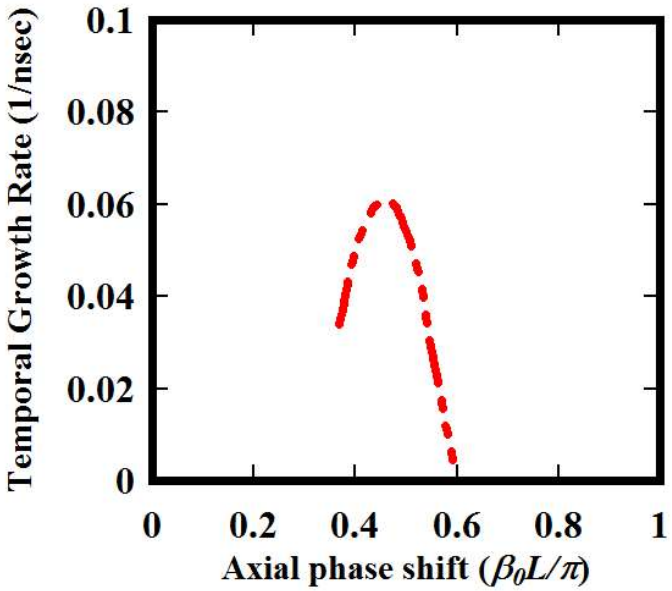

Figure 3.5: Temporal growth rate of periodic SCC structure.

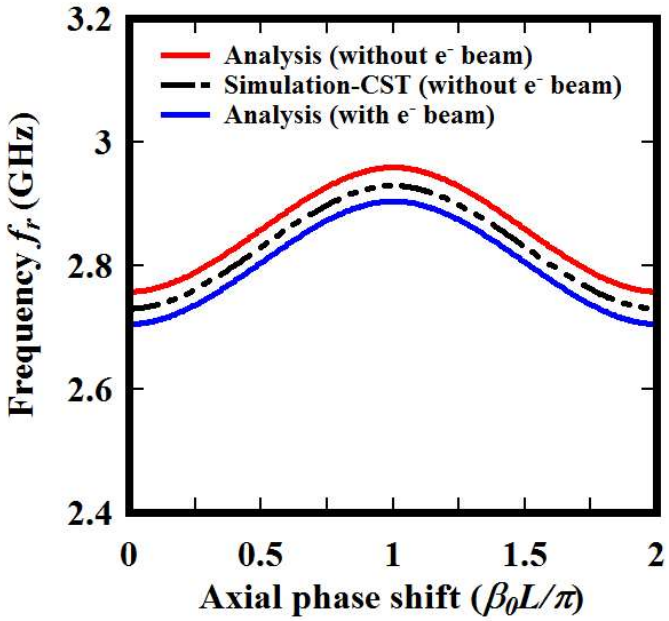

Figure 3.6: Dispersion curve of the periodic SCC structure in the presence and absence of electron beam.

Fig. 3.6 shows the dispersion curve of the periodic SCC structure in the presence and absence of the electron beam. From the figure, it is noted that the dispersion curve associated with the presence of electron beam is decreased as compared to the absence of electron beam. This decrease in the dispersion curve is due to the phenomenon of beam loading which is also known as the beam loading effect.

3.4.1. Parametric Study of the Temporal Growth Rate

The behavior of the temporal growth rate due to the different beam radius has been studied. The effect of different beam radius on the temporal growth rate is shown in Fig. 3.7. From Fig. 3.7, it is observed that the temporal growth rate increases as the beam radius increases (i.e. the instability grows faster with a larger beam radius). This rapid growth in instability occurs due to experiencing a maximum axial electric field near the opening of the cavity by the space-charged sheath [Lemke (1989)].

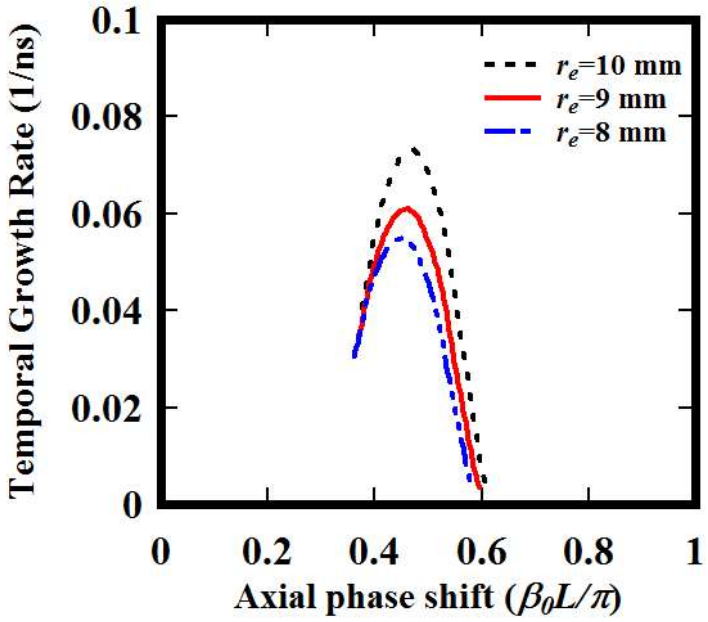

Figure 3.7: Temporal growth rate at different electron beam radius.

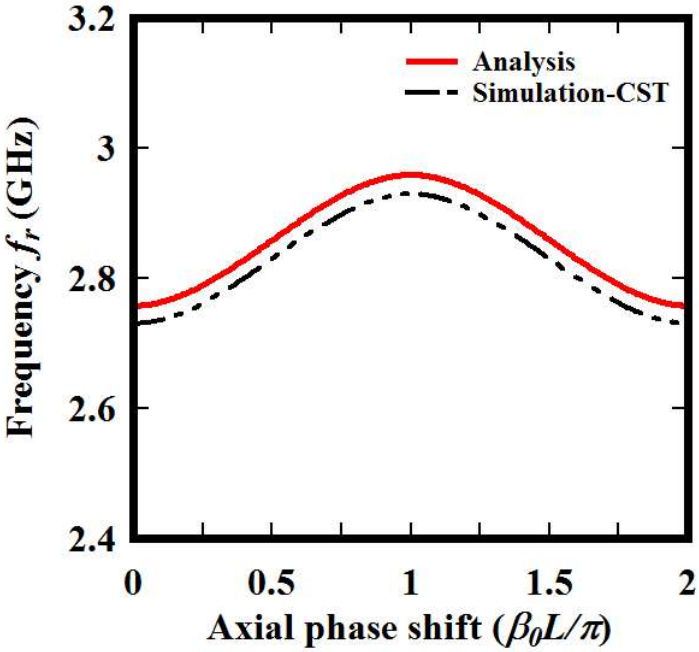

Figure 3.8: Comparison between dispersion curves that have been obtained by simulation and analytical procedure for the special case (i.e. $r_e = 0$).

3.4.2. Validation of the Derived Analytical Relation

Since no research study has been reported for the behavior of SCC in the presence of electron beam, therefore, to validate and verify the preciseness of the derived analysis, the analytically obtained dispersion curve is compared with the dispersion curve obtained from the simulation for the special case i.e. for the zero beam current $(r_e = 0)$. For this special case, the beam presence SCC structure simply converted into the beam absence SCC structure. For the beam absence SCC structure, the dispersion relation is obtained by using EM simulation tool i.e. "CST Studio Suite". The model of the structure is designed according to the structural specification mentioned in the above literature. The dispersion relation obtained through simulation and the derived analysis for the special case (i.e. for

the zero beam current ($r_e = 0$)) is shown in Fig. 3.8. From the Figure, it can be seen that the relative error between the simulated and derived analytical analysis is below 5%, which validates the derived analysis.

3.5. Conclusion

In this chapter, the SCC structure has been analyzed in the presence of an electron beam for its dispersion characteristics using the field matching approach. Since the structure finds its application as a beam-wave interaction cavity in a highly efficient reltron oscillator. Also, the SCC structure has the potential to be used as a beam wave interaction cavity in various slow-wave microwave oscillators such as transit time oscillator, backward wave oscillator, traveling wave tubes, etc. The SCC structure has been investigated for the dispersion behavior and the behavior of the temporal growth rate. Apart from these, the behavior of the temporal growth rate with different beam radii has also been studied. To validate the preciseness of the derived analysis, the analytically obtained dispersion curve has been compared with the dispersion curve obtained from the simulation for the special case (i.e. $r_e = 0$). The purpose of this analysis is to develop a better understanding of the SCC structure and reduce its design complexity.